Glycoconjugate Journal
https://doi.org/10.1007/s10719-021-10020-0

ORIGINAL ARTICLE

Cross-reactivity of *Haemophilus influenzae* type a and b polysaccharides: molecular modeling and conjugate immunogenicity studies

Nicole I. Richardson[1] · Michelle M. Kuttel[2] · Frank St. Michael[3] · Chantelle Cairns[3] · Andrew D. Cox[3] · Neil Ravenscroft[1]

Received: 11 June 2021 / Revised: 16 August 2021 / Accepted: 25 August 2021

Abstract
Haemophilus influenzae is a leading cause of meningitis disease and mortality, particularly in young children. Since the introduction of a licensed conjugate vaccine (targeting the outer capsular polysaccharide) against the most prevalent serotype, *Haemophilus influenzae* serotype b, the epidemiology of the disease has changed and *Haemophilus influenzae* serotype a is on the rise, especially in Indigenous North American populations. Here we apply molecular modeling to explore the preferred conformations of the serotype a and b capsular polysaccharides as well as a modified hydrolysis resistant serotype b polysaccharide. Although both serotype b and the modified serotype b have similar random coil behavior, our simulations reveal some differences in the polysaccharide conformations and surfaces which may impact antibody cross-reactivity between these two antigens. Importantly, we find significant conformational differences between the serotype a and b polysaccharides, indicating a potential lack of cross-reactivity that is corroborated by immunological data showing little recognition or killing between heterologous serotypes. These findings support the current development of a serotype a conjugate vaccine.

Keywords *Haemophilus influenzae* type a · Capsular polysaccharide · Conformation · Cross protection · Molecular modeling · Immunogenicity

Introduction

Haemophilus influenzae is a Gram-negative coccobacillus that is a leading cause of meningitis, otitis media, bacteremia, and pneumonia, amongst others, particularly in children younger than five and immune-compromised individuals, with high levels of morbidity and disability [1–4]. There are six encapsulated serotypes, a – f, based on the capsular polysaccharide (CPS) structure as well as unencapsulated, non-typeable *H. influenzae* (NTHi) strains [1, 5, 6]. *H. influenzae* type b (Hib) was the leading cause of invasive *H. influenzae* disease prior to the introduction of conjugate vaccines in the 1980s and 1990s [2, 3, 7, 8]. The successful introduction of Hib vaccination in many regions has changed the epidemiology of *H. influenzae* disease and resulted in the near elimination of Hib disease. Most invasive disease is now caused by non-b serotypes and NTHi strains, with Hia appearing as a leading cause of disease in Indigenous children in North America [1–3, 8–10]. The emergence of Hia disease despite widespread Hib vaccination suggests that Hib does not cross-protect against Hia and is the motivation for development of a Hia conjugate vaccine. This is aligned with the WHO priority in their "Defeating meningitis by 2030: a global roadmap", particularly as the distribution and burden of disease is underestimated in low- and middle-income countries (LMICs) [4, 6, 9].

Licensed conjugate vaccines against Hib—based on the immunogenic CPS conjugated to different carrier proteins—are available and implemented in national immunization

This article is part of Topical Collection on *Glycoconjugate vaccines: classic and novel approaches*

✉ Neil Ravenscroft
neil.ravenscroft@uct.ac.za

[1] Department of Chemistry, University of Cape Town, Rondebosch 7701, South Africa

[2] Department of Computer Science, University of Cape Town, Rondebosch 7701, South Africa

[3] Vaccine and Emerging Infections Research, Human Health Therapeutics Research Centre, National Research Council, Ottawa, ON K1A 0R6, Canada

Published online: 07 September 2021

programs of all countries except for China and the Russian Federation [4, 11, 12]. For Hia, a promising candidate conjugate vaccine—which is expected to be cost effective in affected areas—has been developed and tested in preclinical studies; it showed immunogenicity, functional antibody stimulation (by serum bactericidal assay), and protective titers equivalent to that of the PedVaxHIB® vaccine (OMPC carrier) [2, 8, 10, 13, 14]. A North American consortium including researchers at McGill University, Dalhousie University, National Research Council, Canadian Immunisation Research Network, Canadian Glycomics Network and Inventprise LLC has identified funds to support GMP clinical lot production, GLP-toxicology studies and a Phase 1 clinical trial of the candidate Hia conjugate vaccine that is scheduled to take place in 2022 [A. Cox, personal communication].

The disaccharide repeating unit structures of the Hib and Hia CPS are similar. The Hib repeating unit (RU)—also commonly known as known as polyribosylribitolphosphate (PRP)—contains ribose, in the β-furanose form, (Rib*f*) as well as ribitol phosphate (Rib-ol) linked by a 1,5-phosphodiester bond (Fig. 1a), whereas Hia contains β-glucopyranose (Glc) and Rib-ol linked via a 4,5-phosphodiester bond (Fig. 1c) [15, 16]. Ribitol phosphate is not present in the CPS of the other *H. influenzae* serotypes [5, 17].

Hib vaccines have poor stability due to the susceptibility of the PRP to hydrolytic cleavage of the phosphodiester bond through nucleophilic attack from O2 of Rib*f* – which

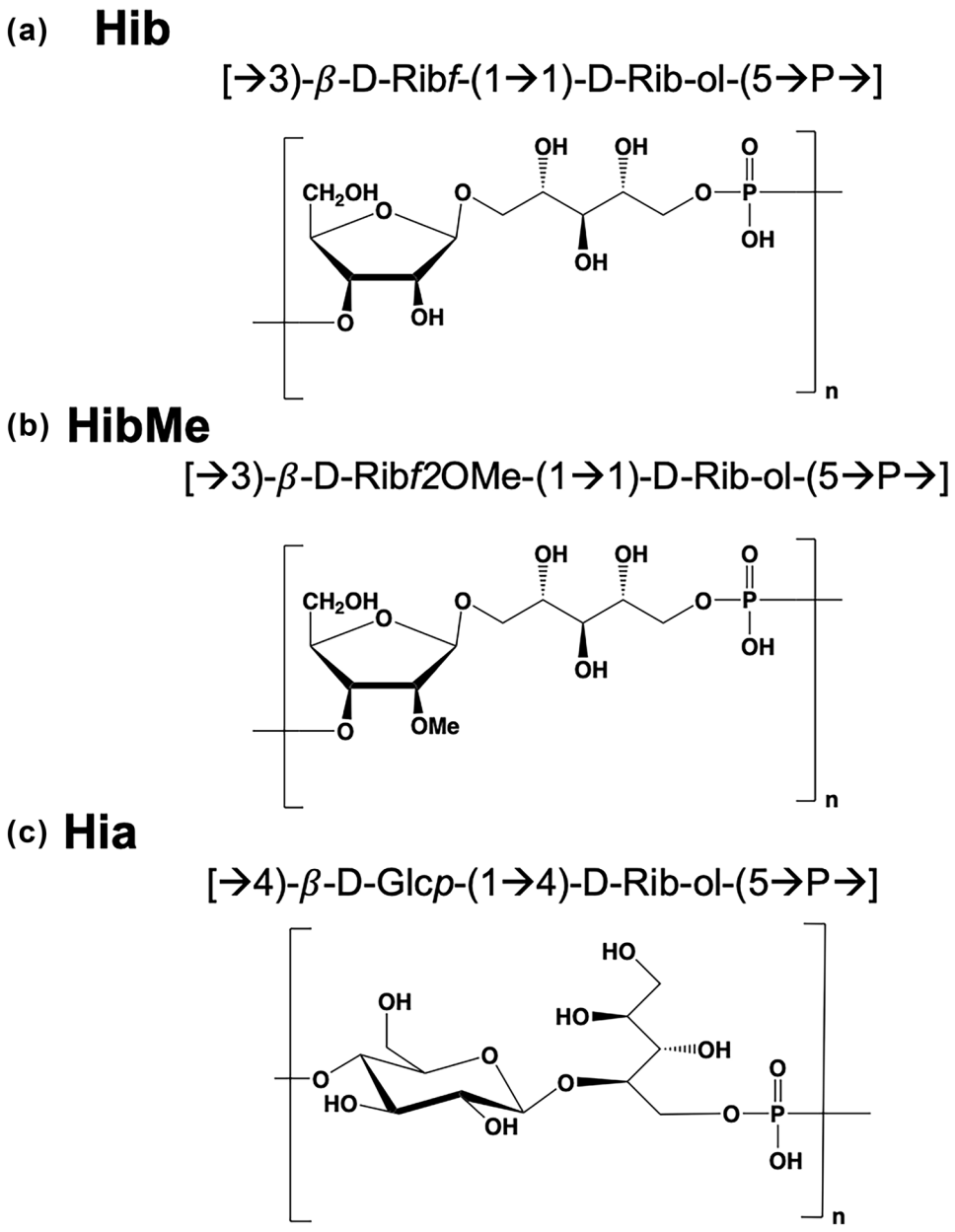

Fig. 1 Primary line structures and repeating units of the CPS modeled in this work: (**a**) *H. influenzae* type b (Hib), (**b**) non-biological stabilized Hib with a methyl group at O2 of Rib*f*, (**c**) *H. influenzae* type a [5, 16, 17, 23, 24]

is further catalyzed by the presence of divalent cations and some adjuvants [18–20]. This must be circumvented when designing the purification of the CPS, its conjugation and, particularly, its formulation in liquid combination vaccines [21]. One solution could be the use of a stabilized Hib antigen. The first example of a conjugate vaccine with a fully synthetic carbohydrate moiety is the QuimiHib made in Cuba [4, 11, 12]; more recently a modular synthetic route was proposed which identified an octasaccharide lead vaccine candidate [22]. The same group showed that methylation at O2 of Rib*f* (see Fig. 1b, HibMe) provides a method for preventing hydrolytic cleavage, thus improving vaccine stability even in the presence of basic aqueous media or aluminum salts, as well as at elevated temperatures, while still inducing an immune response against Hib [19, 20].

As cross-protection between antigens is expected to require both chemical and conformational similarity [23], molecular modeling can provide insight into the potential for cross-protection between the *H. influenzae* CPSs and stabilized Hib. While the structures of *H. influenzae* type a and b polysaccharides have been fully characterized through wet-chemical assays and NMR [16, 24–27], conformational studies have been limited. Physicochemical studies of Hib CPS and a size-reduced activated intermediate showed that Hib behaves as highly flexible random coil [28]. Two decades ago, short molecular dynamics (MD) simulations of one RU of the Hib CPS showed a very flexible phosphodiester linkage [27, 29]. To date, we are not aware of any conformational studies on CPS of Hia or methyl stabilized Hib (HibMe).

To provide insight into potential cross-reactivity between the antigens, in this work we ran microsecond MD simulations of 6 RU of Hib as well as the vaccine candidates Hia and HibMe (Fig. 1) in order to compare the flexibility and dominant conformations of the polysaccharide chains. For experimental corroboration, we also investigated the cross-reactivity between Hib and Hia by performing immunological studies in rabbits.

Methods

Molecular simulations

We used our established systematic approach to the modeling of polysaccharides, as follows [30, 31]. We ran Molecular Dynamics (MD) simulations in solution for CPS chains of 3RU (data not shown) and 6 RU. Chain length is an important consideration when modeling CPSs, as a short chain may have insufficient molecular flexibility, while long chains are more computationally expensive to model. Antibodies have been shown to only bind small fragments of the CPS between one and seven residues in length corresponding to 1–4 RU in the case of *H. influenzae* [32]. Further, native *H. influenzae* CPS is very large and typically sized reduced for use in conjugate vaccines, with 5RU considered sufficient to induce immunity against Hib [11, 22, 33].

Following initial system equilibration, molecular dynamics runs of 1.3 μs were performed and data analyses were performed on these production runs.

Molecular dynamics

Simulations were run using NAMD (version 2.13) [34] with CUDA extensions for graphics processor acceleration [35]. The CHARMM36 additive force field used to model the carbohydrates [36, 37] and TIP3P to model the water molecules [38]. To represent missing glycosidic linkages, we added patches to the CHARMM36 force field for carbohydrates, as well as the necessary bond, angle and dihedral parameters. These were copied from similar linkages in the existing force field. Meso-ribitol, which has a number of alditols, is available in the CHARMM carbohydrate force field. Phosphodiester linkage parameters were adapted from those we previously added to the force field [39]. The initial coordinate files (.pdb format) and associated molecular force field files (protein structure file format, .psf) for all systems modeled are provided as online resources 1–6.

Starting structures for each molecule (Fig. 1 and Fig. S1) were built with CarbBuilder [40] using the default glycosidic linkages designated by CarbBuilder: for the β-linkages φ, ψ = 40, 0 and for the phosphodiester linkages φ, ψ = -40, 0. These initial structures were then minimized with NAMD for 10 000 steps at 300 K.

Minimized structures were solvated using the Visual Molecular Dynamics (VMD) software [41] to add cubic water boxes of 60 Å per side for Hib/HibMe and 72 Å per side for Hia. Each system was ionized with sodium (Na^+) counter ions to neutralize the system (3 ions for the 3RU, 6 for the 6 RU) at an ionic concentration of 0.027 mol/L and 0.046 mol/L for the 72 Å and 60 Å boxes respectively. Initial minimization and heating protocols comprised 5 K incremental temperature reassignments beginning at 10 K up to 300 K with 5 000 steps of NAMD minimization and 2 000 steps of MD at each temperature reassignment.

Periodic boundary conditions equivalent to the cubic box size were employed for the solvated simulation with wrapping on. Long range electrostatics were implemented with Particle Mesh Ewald summation (PME) on a 60 Å (Hib/HibMe) or 72 Å (Hia) grid size [42]. Atoms were not held fixed, and the initial center of mass motion was off. The 1–3 pairs were excluded from non-bonded interactions, 1–4 interactions were not scaled, and the dielectric constant was set to 1. Smoothing functions were applied to both the electrostatics and van der Waals forces with switching and cutoff distances of 12 Å and 15 Å, respectively.

A Leap-Frog Verlet integrator was used to integrate the equations of motion over a step size of 1 fs. A distance of 18 Å was used as the cut-off for inclusion in the pair list for calculation of non-bonded forces. The short-range non-bonded interactions were calculated every 1 fs, full electrostatics calculations were performed every 2 fs, and atoms were reassigned every 10 fs [43].

Simulations were sampled under isothermal-isobaric (nPT) ensemble. Langevin dynamics were used to control the temperature with a damping coefficient of 5/ps. Nosé-Hoover Langevin piston dynamics were used as a barostat to maintain a target pressure of 1 atm. Variable system volume was used with a piston period of 100 fs and decay of 50 fs. Post equilibration (200 ns), simulations underwent production runs of 1300 ns as was required for the different models to converge.

Convergence

We addressed convergence using block standard averaging [44] applied to two metrics: end-to-end distance and radius of gyration (Supplementary Fig. S2). Block standard averaging was implemented with in-house Python scripts, as previously described [30, 44].

For all simulations, the blocked standard error (BSE) reached plateaus for both metrics, indicating convergence. The simulation lengths were large multiples of the correlation times for end-to-end distance (Hib, 11 ns; HibMe, 11 ns; Hia, 24 ns) and radius of gyration (Hib, 11 ns; HibMe, 11 ns; Hia, 25 ns). Further, the numbers of independent samples were $>>1$ for both the end-to-end distance (Hib, 143; HibMe, 131; Hia, 64) and the radius of gyration (Hib, 131; HibMe, 142; Hia, 60). Our designated equilibration time of 200 ns is therefore much greater than the correlation time.

Data analysis

Output trajectories were extracted every 25 ps and analyzed at 250 ps intervals. Inter-atomic distances and dihedral angles were measured using VMD, with data analyses performed with in-house Python scripts and plots generated using Matplotlib [45].

The end-to-end distance, *r*, was measured from C1 of Rib-ol at the non-reducing end, to C1 of Rib*f* (for Hib) or Glc (for Hia) at the reducing end, thus excluding the highly flexible terminal residues.

The glycosidic linkages Rib*f*(11)Rib-ol and Glc*p*(14) Rib-ol are described by two dihedral angles $\varphi = $ H1-C1-O1-C_x' and $\psi = $ C1-O1-C_x'-H_x', which are equivalent to φ_H and ψ_H in IUPAC nomenclature [46, 47]. The phosphodiester linkages were defined as: $\varphi = H_x\text{-}C_x\text{-}O_x\text{-}P$, $\psi = C_x\text{-}O_x\text{-}P\text{-}O_y$, $\omega = O_x\text{-}P\text{-}O_y\text{-}C_y$ and $\varepsilon = P\text{-}O_y\text{-}C_y\text{-}H_y$ as we have previously done for this type of linkage [48]. All dihedral angles were measured as a combination of the dihedrals from the central RUs, three and four thus providing a sample of the most central angles.

The most common chain conformations for each simulation were determined by clustering the simulations frames (post equilibration) into families and calculating the relative occupancies of each family. Clusters comprising less than 2% of the production run (post equilibration) were discarded. Clustering was performed using the WMC PhysBio plug-in for VMD's built-in cluster command [49]. Prior to clustering, the molecules were aligned on the ring and linkage atoms of the central Rib-ol residue of RU 3 and Rib*f* residue of RU 4. Clustering was performed as an RMSD fit to the ring and linkage atoms of the central 4 RU of the 6 RU chains (excluding the highly flexible terminal repeating units) with a cut-off of 5.5 Å.

Hydrophilic/hydrophobic regions of the molecular surface were analyzed using VMD's built in "measure sasa" command. The solvent accessible surface area (sasa) analysis was performed by probing first hydrophilic regions (comprising hydroxyl groups, carbonyl groups, ring oxygens, phosphorous, and linkage oxygens) and then hydrophobic/neutral regions (comprising methyl groups, CH_2 groups, ring carbons, and ring protons) of the molecule using a van der Waal's radius of 1.4 Å—analogous to that of water. The ratio of hydrophilic to hydrophobic/neutral regions was then calculated to determine the percentage hydrophilic surface area available for potential antibody binding.

Molecular conformations were visualized using VMD, with the PaperChain visualization algorithm used to highlight carbohydrate rings [50]. and the hydrophilic and hydrophobic surfaces were visualized with the Quicksurf visualization algorithm [51].

Immunological studies

CPS from Hia and Hib were isolated from cell supernatants following fermenter growth, as described previously for Hia, however, no RNase treatment was utilized for Hib CPS isolation [8]. CRM_{197} carrier protein was prepared as described previously [8]. Conjugates of purified Hia and Hib CPS were prepared via direct reductive amination as described previously for the Hia conjugates [8].

Three New Zealand female white rabbits (Hia: RCAV1-3), (Hib: RCBV1-3) were immunized sub-cutaneously with each conjugate at a 25 µg dose with the same prime and two boost strategy and adjuvanting with incomplete Freund's adjuvant as described previously [8].

Final bleed day 70 (D70) rabbit sera from Hia and Hib conjugates were screened against BSA conjugates of Hia and Hib PS in ELISA as described previously [8]. Pre-immune sera were employed as the negative control.

Final bleed (D70) rabbit sera from Hia and Hib conjugates were screened for functionality in a serum bactericidal assay (SBA) against Hia strain (NRCC # 6753) and Hib strain (NRCC # 4274) as described previously [8]. Pre-immune sera were employed as the negative control.

Results

We begin with a comparison of the flexibilities of the Hib, HibMe, and Hia CPS chains, then the molecular conformations, followed by the minimal binding epitopes and the characteristics of the molecular surface. We then discuss the results of our immunological studies in the light of the modeling results.

Chain flexibility

Time series graphs of the molecular end-to-end distance, *r*, over the course of the MD simulations provide a simple metric for comparison of the molecular flexibility and extension of the 6 RU CPS chains. The *r* time series plots (Fig. 2, left column) and corresponding histograms (Fig. 2, right column) reveal that all three molecules are very flexible,

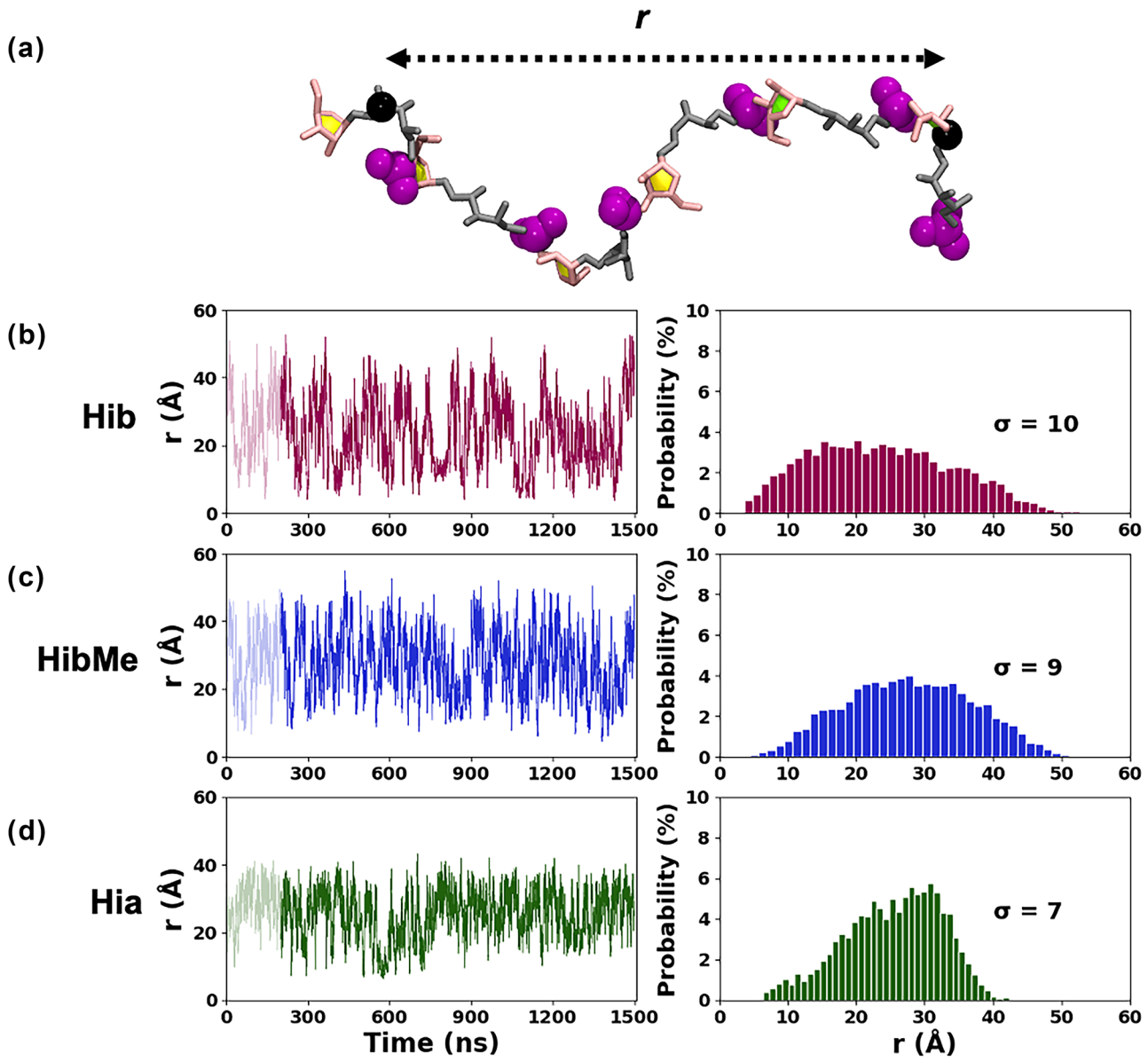

Fig. 2 Time series of the end-to-end distance, *r*, in the 6 RU CPS chains. Here *r* is defined as the distance (Å) from C1 of Rib-ol in RU 1 to C1 of Rib*f* in RU 6 for Hib and HibMe (**a**), or the equivalent C1 of Glc in RU 6 (for Hia). Time series (left column) and histograms (right column) are plotted for *r* in (**b**) Hib, (**c**) HibMe, and (**d**) Hia. Histograms are labelled with the standard deviation, σ

with rapid transition between a wide range of *r* values. The similarity of the plots for Hib (Fig. 2b) and HibMe (Fig. 2c) indicate that the O-methyl substitution on Hib does not affect the flexibility of the chain substantially: Hib and HibMe have the same range of *r* (5–55 Å), although the *r* histograms reveal that Hib has a greater incidence of conformations with $r < 10$ Å. However, Hib and HibMe together are considerably more flexible than Hia (Fig. 2d). The range of *r* is considerably broader for Hib and HibMe than for Hia (5–45 Å), which lacks the extreme extensions of the chain. Further, the more compact distribution of Hia ($\sigma = 7$ Å), with a clear peak at approximately 30 Å, indicates that it is more conformationally defined than either Hib ($\sigma = 10$ Å) or HibMe ($\sigma = 9$ Å).

Molecular conformations

The flexibility of the CPS antigens is further demonstrated in a comparison of the dominant CPS chain conformations for Hib, HibMe, and Hia (Fig. 3). Hib has no dominant conformation, with the highest occupation for a conformational family at 7% of simulation time (Fig. 3a, Hib1). The wide range of collapsed (Fig. 3a: Hib1, Hib2, Hib8) and extended (Fig. 3a: Hib3-7 and Hib9-10) conformations with low occupancies (< 7%) for Hib is consistent with the random coil classification of this antigen on the basis of sedimentation studies [28]. The conformations of HibMe (Fig. 3b) are very similar to Hib, although with more extended chain conformations: O-methyl substitution of the Rib*f* residue removes the compact conformations of Hib. However, there remains a wide range of conformations of the chain, which also behaves as a random coil.

In contrast, the conformations of Hia are much more defined and regular (Fig. 3c), with the primary cluster comprising 36% of the simulation (Fig. 3c, Hia1). Zig-zag conformations of the chain predominate (Fig. 3c, Hia1, Hia5, Hia6), with bends at the Rib-ol of each RU. More compact conformations with accordion-style folding of the zig-zag do occur with relatively high frequency (Fig. 3c, Hia2, Hia4, Hia8, Hia9), but very extended conformations of the chain are absent. The glycosidic linkages (Supplementary information, Figs. S3 and S4) in the Hia simulations are more constrained and have different orientations than in Hib. Overall, Hia therefore has markedly different conformations and dynamics to Hib.

Binding epitopes

As the CPS regions bound by antibodies comprise one to seven residues [32], it is useful to compare the 6 RU CPS chains on this length scale. Figure 4 shows the three main conformations of the central 4 RU segment (comprising 2 RU) for the Hib, HibMe, and Hia CPS chains. Overall, the three primary conformations of the 2 RU segments are much more consistent with each other than the conformations of the 6 RU chains.

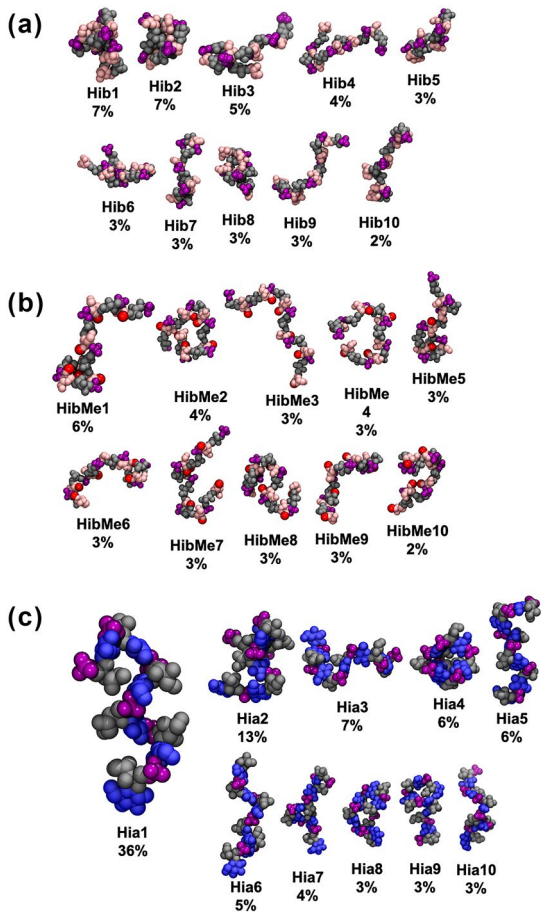

Fig. 3 Conformational families for the middle 4 RU of the 6 RU CPS chains: (**a**) Hib, (**b**) HibMe and (**c**) Hia. Families are scaled to illustrate differences in their relative percentage occupancies. Residues are colored: Rib*f*, pink; Rib-ol, gray; Glc, blue. The phosphate groups are highlighted in purple and the methyls in red

At this scale it is clear that the flexible phosphodiester linkage acts as a hinge between repeating units for all three CPS chains. However, the conformations of the 2 RU segment are quite different across the three antigens. The primary conformations of Hib are compact, with sharp bends exposing the phosphate group (Fig. 4a), whereas the primary conformations for HibMe are more extended, with the O-methyl group quite exposed on the chain (Fig. 4b). For Hib (Fig. 4a) the sharp bends enable conformational collapse and stabilizing interactions between the Rib-ol and opposing sides of the chain (Fig. 4d) likely increase the preference for collapsed over extended conformations in this CPS. For HibMe the bulky methyl group at O2 of Rib*f* prevents collapse and more extended conformations therefore predominate.

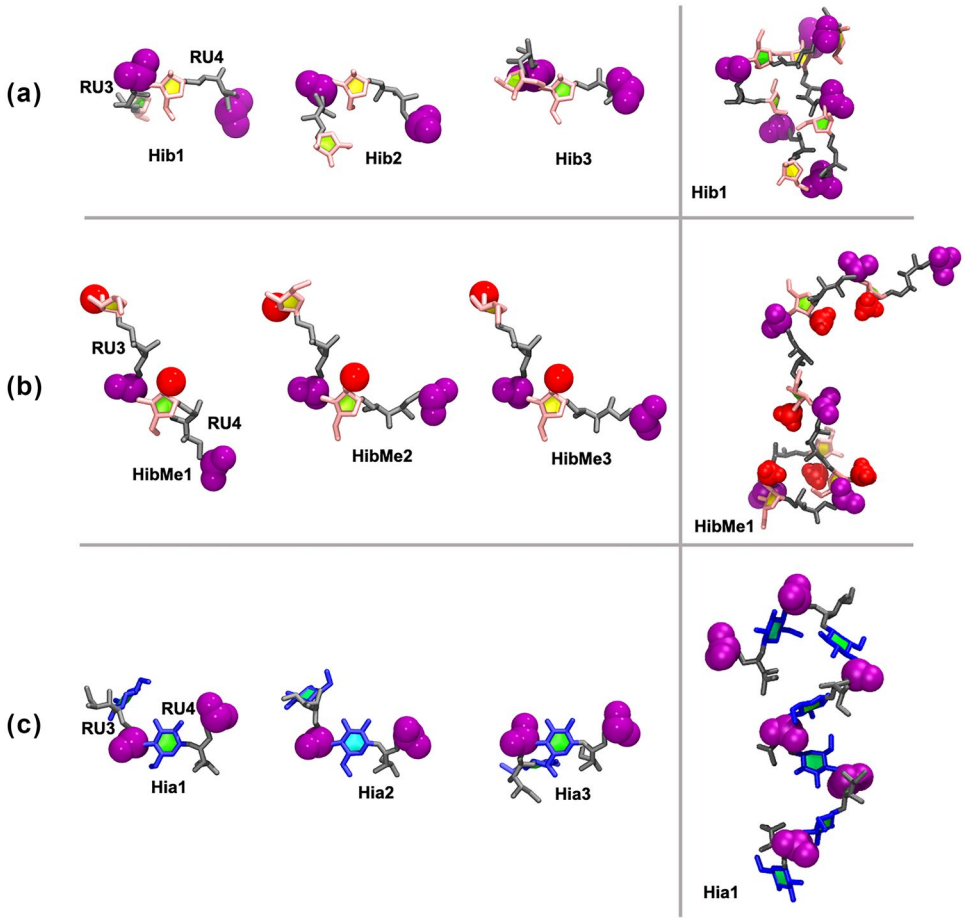

Fig. 4 Four residue sections of the CPS chains comprising RU 3 and RU 4 for the three primary conformational clusters: (**a**) Hib, (**b**) HibMe and (**c**) Hia. The full primary clusters for Hib, HibMe, and Hia are shown in the last column. Residues are colored: Rib*f*, pink; Rib-ol, gray; Glc, blue. The phosphate groups are highlighted in purple and the methyls in red

The more moderate bends in the Hia conformations (Fig. 4c) are due to the constrained 4,5 linked Rib-ol. Here the phosphate hinge exposes both the phosphate groups as well as the bulky C1-C3 portion of the Rib-ol for possible antibody binding (Fig. 4f).

Comparison of the solvent exposed hydrophilic and hydrophobic regions of the molecular surfaces further highlights significant differences between the CPS antigens that may affect antibody binding. Time series and histograms of the solvent exposed hydrophilic surface area for step in the simulation are plotted in Fig. 5. As expected, the surface of the Hib CPS (Fig. 5a) is largely hydrophilic (average of 72%)—due primarily to the bulky charged phosphate groups. However, the addition of the hydrophobic methyl group in HibMe greatly reduces the hydrophilicity of the exposed molecular surface to an average of 57% (Fig. 5b). This can be rationalized by considering that the methyl group in HibMe is relatively bulkier (4 atoms) compared to the OH in Hib (2 atoms), thus the methyl substituent would contribute more to the hydrophobicity of the molecular surface in HibMe than the OH contributes to hydrophilicity of the surface in Hib. In addition to the conformational differences in the chain, this difference in the properties of the surface is another factor to consider that may affect cross-reactivity between the two antigens.

Interestingly, the analysis shows that Hia (Fig. 5c) has the same relative hydrophilicity as Hib, an average of 72% (with a narrower distribution), despite the significant structural and conformational differences between these antigens. This is consistent with a comparison of the hydrophilic surfaces of the Rib*f* (Fig. S5a, 69%) and Glc (Fig. S5b, 69%) residues—which, given the common Rib-ol residue (Fig. S5c) contributes to the overall hydrophilicity of the surface.

Immunological studies

To investigate cross-reactivity between Hib and Hia, D70 rabbit sera derived from immunizations with three doses of the Hia and Hib conjugates were screened in ELISA for recognition of the homologous and heterologous CPS (Fig. 6). Only the homologous CPS was recognized in each case, confirming a lack of cross-reactivity between the Hia and Hib CPS.

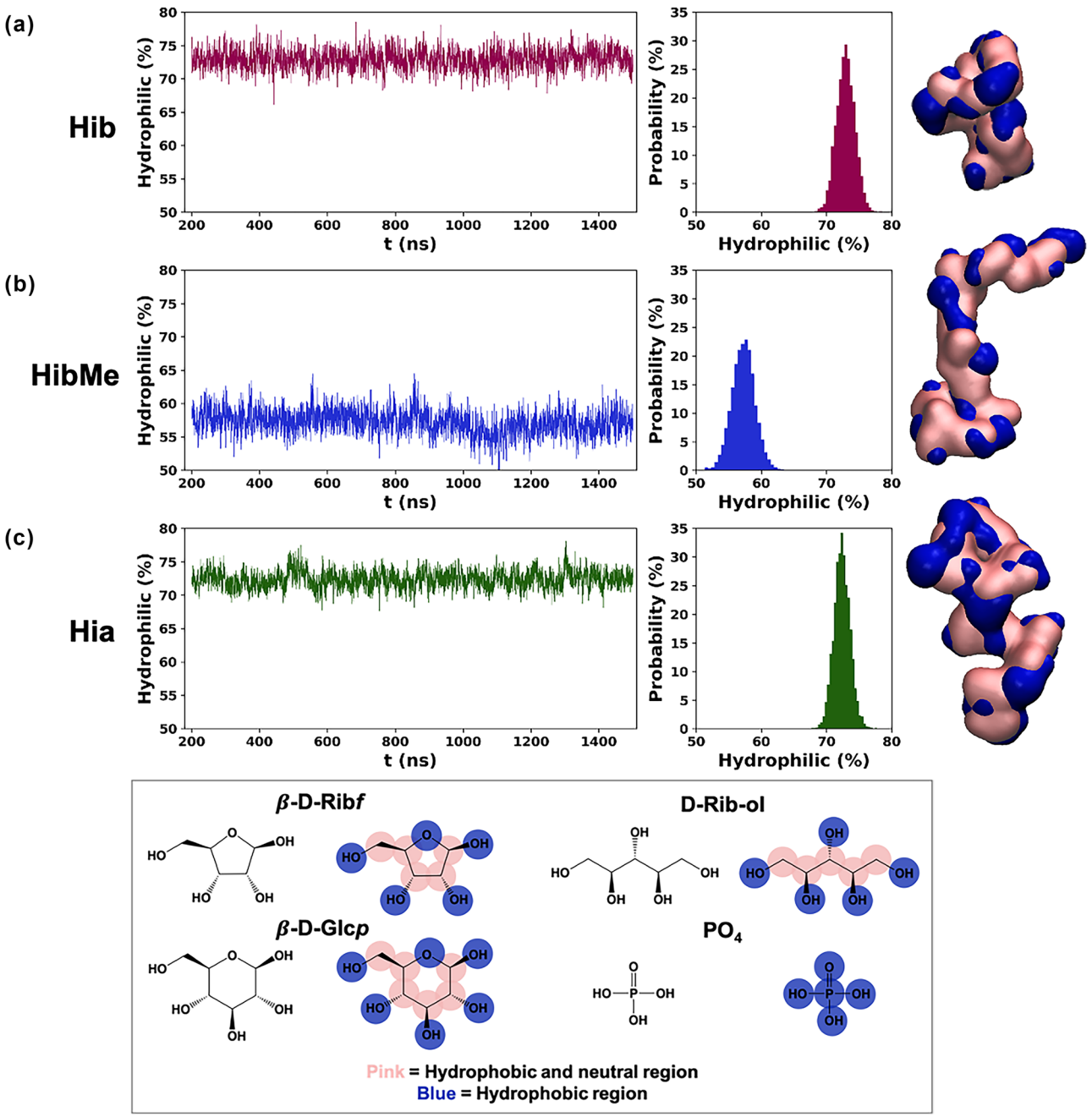

Fig. 5 Time series plots and histograms of the percentage of the solvent accessible surface area that is hydrophilic in the 6 RU simulations of (**a**) Hib, (**b**) HibMe, and (**c**) Hia. Examples of the molecular surfaces for each CPS with hydrophilic (blue) and hydrophobic (pink) patches indicated are shown in the right column; the key and classification for each RU moiety is given in the lower panel

The same D70 sera were utilized in an SBA assay to assess for functionality of the sera that supports complement-mediated killing. As can be seen in Fig. 7, the Hia conjugate derived sera could only facilitate the killing of the Hia strain and not killing of the Hib strain. The same reciprocal results were obtained when the Hib conjugate derived sera were examined, confirming the inability of sera specific to one serotype to recognize nor facilitate the killing of the heterologous serotype strains.

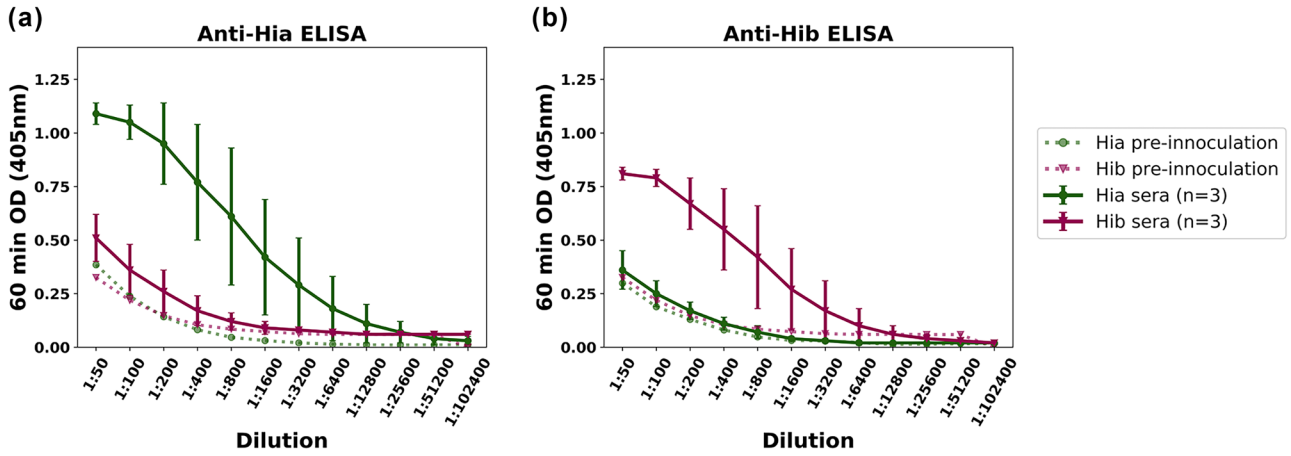

Fig. 6 ELISA screening of rabbit sera from Hia or Hib conjugate immunized rabbits (n = 3) for recognition of: (**a**) Hia-BSA conjugate or (**b**) Hib-BSA conjugate. Homologous serotype recognition is seen, but no cross-recognition of the heterologous serotype. In all cases the pre-immunization sera were used as the control

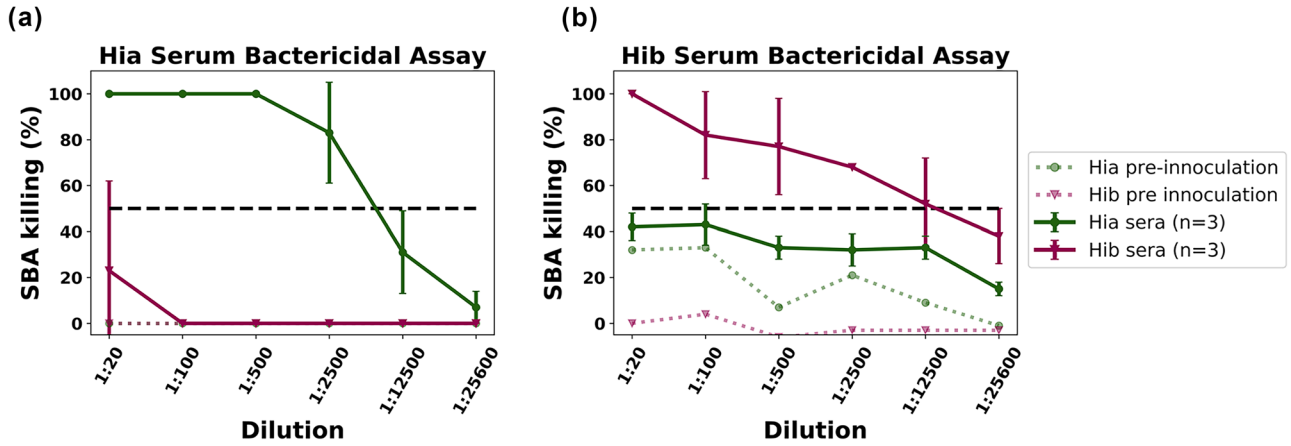

Fig. 7 Serum bactericidal assay (SBA) titration curves of rabbit sera from Hia or Hib conjugate immunized rabbits (n = 3) against: (**a**) Hia bacterial strain # 6753 or (**b**) Hib bacterial strain # 4274. We see killing of the homologous serotype, but a lack of cross-killing of the heterologous serotype. In all cases, pre-immunization sera were used as the control

Discussion

We find that Hib and the modified HibMe CPS antigens both behave as unstructured random coils in solution. However, we show that there are also some differences between the Hib and HibMe saccharides that may affect antibody binding: Hib has a range of collapsed, globular conformations that do not occur in HibMe, the local conformation of the chain in Hib has more extreme bends than HibMe, and the molecular surface of Hib is much more hydrophilic than HibMe. However, despite the differences in conformation and molecular surface, a modified HibMe conjugate vaccine raised antibodies that recognized the natural Hib antigen [19]. This suggests that the presence of immuno-dominant charged phosphate [52] is the focus of antibody recognition and binding.

In contrast to Hib, the flexible Hia CPS forms relatively defined zig-zag conformations. We find significant differences between the Hia and Hib CPS antigens in flexibility, conformation, and minimal binding epitope, which does not support the existence of cross-reactivity between them. The immunological data confirms this: sera derived from Hia CPS conjugates cannot recognize nor kill Hib strains and sera derived from Hib CPS conjugates cannot recognize nor kill Hia strains. This is also consistent with clinical data showing an increase in invasive disease caused by serotype a in infants and children, even after receiving a full childhood serotype b conjugate vaccine regimen [53, 54]. Based on

the limited immunogenicity studies detailed herein, we also note that Hia appears to elicit a stronger immune response than the highly flexible Hib; it is interesting to postulate that the more conformationally defined Hia CPS is a stronger antigen than Hib.

Future work is focused on the development of a Hia glycoconjugate vaccine to protect all infants and children from this disease; funding has been secured for Phase 1 clinical trial of a prospective Hia vaccine by a North American consortium.

Abbreviations BSA: Bovine serum albumin; CPS: Capsular polysaccharide; ELISA: Enzyme-linked immunosorbent assay; Glc: Glucose; Hia: *H. influenzae* Type a; Hib: *H. influenzae* Type b; HibMe: *H. influenzae* Type b methylated at O2 of ribose; PRP: Polyribosylribitolphosphate; Rib*f*: ribose/ribofuranose; Rib-ol: Ribitol phosphate; RU: Repeating unit; SBA: Serum bactericidal assay

Supplementary information The online version contains supplementary material available at https://doi.org/10.1007/s10719-021-10020-0.

Acknowledgements Computations were performed using facilities provided by the University of Cape Town's ICTS High Performance Computing team: http://hpc.uct.ac.za. The authors wish to thank the staff of the NRC-Ottawa animal facility who carry out all animal work following NRC's Human Health Therapeutics Research Centre's animal care committee approved procedures that fall under the Canadian Council of Animal Care jurisdiction

Authors' contributions Conceptualization, M.M.K and N.R; methodology, M.M.K; software, M.M.K and N.I.R; validation, M.M.K and N.I.R; investigation, N.I.R., F.S.M and C.C; resources, M.M.K. and N.R; data curation, M.M.K; writing—original draft preparation, A.C. and N.I.R.; writing—review and editing, M.M.K and N.R; supervision, A.C, M.M.K and N.R; visualization, M.M.K and N.I.R.; funding acquisition, M.M.K and N.R.

Funding This research was partially funded by the University of Cape Town (MSc scholarship for N.I.R).

Data availability All data has been disclosed.

Code availability Not applicable.

Compliance with ethical standards

Conflicts of interest The authors declare that they have no conflicts of interest.

Ethical approval This article does not contain any studies with human participants or animals performed by any of the authors.

References

1. Tsang, R.S.W., Ulanova, M.: The changing epidemiology of invasive Haemophilus influenzae disease: Emergence and global presence of serotype a strains that may require a new vaccine for control. Vaccine (2017). https://doi.org/10.1016/j.vaccine.2017.06.001
2. Barreto, L., Cox, A.D., Ulanova, M., Bruce, M.G., Tsang, R.: The emerging Haemophilus influenzae serotype a infection and a potential vaccine: Implementation science in action. Can. Commun. Dis. Rep. (2017). https://doi.org/10.14745/ccdr.v43i05a01
3. Slack, M.P.E.: Long Term Impact of Conjugate Vaccines on Haemophilus influenzae Meningitis: Narrative Review. Microorganisms (2021). https://doi.org/10.3390/microorganisms9050886
4. World Health Organization: Defeating Meningitis by 2030: global road map. https://www.who.int/initiatives/defeating-meningitis-by-2030. Accessed 03 May 2021
5. Kenne, L., Lindberg, B.: The Polysaccharides. In: Aspinall, G.O. (ed.) The polysaccharides, pp. 287–363. Academic Press (1983)
6. Ulanova, M.: Invasive Haemophilus influenzae Serotype a Disease in the H. influenzae Serotype b Conjugate Vaccine Era: Where Are We Going?. Clin. Infect. Dis. (2020). https://doi.org/10.1093/cid/ciaa868
7. Zwahlen, A., Kroll, J.S., Rubin, L.G., Moxon, E.R.: The molecular basis of pathogenicity in Haemophilus influenzae: comparative virulence of genetically-related capsular transformants and correlation with changes at the capsulation locus cap. Microb. Pathog. (1989). https://doi.org/10.1016/0882-4010(89)90058-2
8. Cox, A.D., Williams, D., Cairns, C., Michael, F.S., Fleming, P., Vinogradov, E., Arbour, M., Masson, L., Zou, W.: Investigating the candidacy of a capsular polysaccharide-based glycoconjugate as a vaccine to combat Haemophilus influenzae type a disease: a solution for an unmet public health need. Vaccine (2017). https://doi.org/10.1016/j.vaccine.2017.09.055
9. Ulanova, M., Tsang, M.D., Raymond S.W, Dr: Haemophilus influenzae serotype a as a cause of serious invasive infections. Lancet Infect. Dis. (2014). https://doi.org/10.1016/S1473-3099(13)70170-1
10. Cox, A.D., Lee, R.K., Ulanova, M., Bruce, M.G., Tsang, R.: Proceedings of a workshop to discuss the epidemiology of invasive Haemophilus influenzae disease with emphasis on serotype a and b in the Americas, 2019. Vaccine (2021). https://doi.org/10.1016/j.vaccine.2020.12.015
11. Verez-Bencomo, V., Fernandez-Santana, V., Hardy, E., Toledo, M.E., Rodríguez, M.C., Heynngnezz, L., Rodriguez, A., Baly, A., Herrera, L., Izquierdo, M.: A synthetic conjugate polysaccharide vaccine against Haemophilus influenzae type b. Science (2004). https://doi.org/10.1126/science.1095209
12. Zarei, A.E., Almehdar, H.A., Redwan, E.M.: Hib Vaccines: Past, Present, and Future Perspectives. J. Immunol. Res. (2016). https://doi.org/10.1155/2016/7203587
13. Cox, A.D., Barreto, L., Ulanova, M., Bruce, M.G., Tsang, R.: Implementation science: Developing a vaccine for Haemophilus influenzae serotype a: Proceedings of a workshop. Can. Commun. Dis. Rep. (2017). https://doi.org/10.14745/ccdr.v43i05a02
14. Shoukat, A., Van Exan, R., Moghadas, S.M.: Cost-effectiveness of a potential vaccine candidate for Haemophilus influenzae serotype 'a.' Vaccine (2018). https://doi.org/10.1016/j.vaccine.2018.01.047
15. Lemercinier, X., Jones, C.: An NMR Spectroscopic Identity Test for the Control of the Capsular Polysaccharide from Haemophilus influenzae Type b. Biologicals (2000). https://doi.org/10.1006/biol.2000.0255
16. Egan, W., Schneerson, R., Werner, K.E., Zon, G.: Structural studies and chemistry of bacterial capsular polysaccharides. Investigations of phosphodiester-linked capsular polysaccharides isolated from Haemophilus influenzae types a, b, c, and f: NMR spectroscopic identification and chemical modification of end groups and the nature of base-catalyzed hydrolytic depolymerization. J. Am. Chem. Soc. (1982). https://doi.org/10.1021/ja00374a033
17. Ovodov, Y.: Bacterial capsular antigens. Structural patterns of capsular antigens. Biochemistry (2006). https://doi.org/10.1134/S000629790609001X
18. Sturgess, A.W., Rush, K., Charbonneau, R.J., Lee, J.I., West, D.J., Sitrin, R.D., Hennessey, J.P., Jr.: Haemophilus influenzae type b

conjugate vaccine stability: catalytic depolymerization of PRP in the presence of aluminum hydroxide. Vaccine (1999). https://doi.org/10.1016/S0264-410X(98)00337-5
19. Emmadi, M., Lisboa, M.P., Monnanda, B, Sharavathi, G., Parameswarappa, S., Oestreich, S., Nieto-Garcia, O., Seeberger, P.H., Von Bonin, A., Pereira, C.L.: A Liquid Stable Biological Active Semi-Synthetic Glycoconjugate Vaccine against Haemophilus influenzae type b
20. Seeberger, P.H., Pereira, C.L.: Stable hydrolysis-resistant synthetic polyribosylribitolphosphate derivatives as a vaccine against Haemophilus influenzae type B, USA, Patent Number: US20190153015A1 (2019).
21. Hennessey Jr, J.P., Costantino, P., Talaga, P., Beurret, M., Ravenscroft, N., Alderson, M.R., Zablackis, E., Prasad, A.K., Frasch, C.: Lessons learned and future challenges in the design and manufacture of glycoconjugate vaccines. In: Prasad, A.K. (ed.) Carbohydrate-Based Vaccines: From Concept to Clinic, pp. 323–385. ACS Publications (2018)
22. Baek, J.Y., Geissner, A., Rathwell, D.C.K., Meierhofer, D., Pereira, C.L., Seeberger, P.H.: A modular synthetic route to size-defined immunogenic Haemophilus influenzae b antigens is key to the identification of an octasaccharide lead vaccine candidate. Chem. Sci. (2018). https://doi.org/10.1039/c7sc04521b
23. Kuttel, M.M., Ravenscroft, N.: The Role of Molecular Modeling in Predicting Carbohydrate Antigen Conformation and Understanding Vaccine Immunogenicity. In: Prasad Krishna, A. (ed.) Carbohydrate-Based Vaccines: From Concept to Clinic, pp. 139–173. ACS Publications (2018)
24. Byrd, R.A., Egan, W., Summers, M.F., Bax, A.: New N.M.R.-spectroscopic approaches for structural studies of polysaccharides: Application to the Haemophilus influenzae type a capsular polysaccharide. Carbohydr. Res. (1987). https://doi.org/10.1016/0008-6215(87)80043-5
25. Branefors-Helander, P., Kenne, L., Lindberg, B., Petersson, K., Unger, P.: Structural studies of two capsular polysaccharides elaborated by different strains of Haemophilus influenzae type e. Carbohydr. Res. (1981). https://doi.org/10.1016/S0008-6215(00)84602-9
26. Branefors-Helander, P., Kenne, L., Lindberg, B., Petersson, K., Unger, P.: Structural studies of the capsular polysaccharide elaborated by Haemophilus influenzae type d. Carbohydr. Res. (1981). https://doi.org/10.1016/S0008-6215(00)80674-6
27. Hoog, C., Laaksonen, A., Widmalm, G.: Molecular dynamics simulations of the phosphodiester-linked repeating units of the Haemophilus influenzae types c and f capsular polysaccharides. J. Phys. Chem. B (2001). https://doi.org/10.1021/jp0041555
28. Abdelhameed, A.S., Adams, G.G., Morris, G.A., Almutairi, F.M., Duvivier, P., Conrath, K., Harding, S.E.: A glycoconjugate of Haemophilus influenzae Type b capsular polysaccharide with tetanus toxoid protein: hydrodynamic properties mainly influenced by the carbohydrate. Sci. Rep. (2016). https://doi.org/10.1038/srep22208
29. Maestre, M., Pérez, C.S.: Conformational analysis of diribosylribitol phosphate by NMR spectroscopy and molecular dynamics. Magn. Reson. Chem. (2000). https://doi.org/10.1002/(SICI)1097-458X(200002)38:23.0.CO;2-L
30. Hlozek, J., Owen, S., Ravenscroft, N., Kuttel, M.M.: Molecular Modeling of the Shigella flexneri Serogroup 3 and 5 O-Antigens and Conformational Relationships for a Vaccine Containing Serotypes 2a and 3a. Vaccines (2020). https://doi.org/10.3390/vaccines8040643
31. Richardson, N.I., Ravenscroft, N., Arato, V., Oldrini, D., Micoli, F., Kuttel, M.M.: Conformational and Immunogenicity Studies of the Shigella flexneri Serogroup 6 O-Antigen: The Effect of O-Acetylation. Vaccines (2021). https://doi.org/10.3390/vaccines9050432
32. Kabat, E.A.: The nature of an antigenic determinant. J. Immunol. (1966)
33. Ravenscroft, N., Averani, G., Bartoloni, A., Berti, S., Bigio, M., Carinci, V., Costantino, P., D'Ascenzi, S., Giannozzi, A., Norelli, F., Pennatini, C., Proietti, D., Ceccarini, C., Cescutti, P.: Size determination of bacterial capsular oligosaccharides used to prepare conjugate vaccines. Vaccine (1999). https://doi.org/10.1016/S0264-410X(99)00092-4
34. Phillips, J.C., Braun, R., Wang, W., Gumbart, J., Tajkhorshid, E., Villa, E., Chipot, C., Skeel, R.D., Kale, L., Schulten, K.: Scalable molecular dynamics with NAMD. J. Comput. Chem. (2005). https://doi.org/10.1002/jcc.20289
35. Stone, J.E., Phillips, J.C., Freddolino, P.L., Hardy, D.J., Trabuco, L.G., Schulten, K.: Accelerating molecular modeling applications with graphics processors. J. Comput. Chem. (2007). https://doi.org/10.1002/jcc.20829
36. Guvench, O., Greene, S.N., Kamath, G., Brady, J.W., Venable, R.M., Pastor, R.W., Mackerell, A.D., Jr.: Additive empirical force field for hexopyranose monosaccharides. J. Comput. Chem. (2008). https://doi.org/10.1002/jcc.21004
37. Guvench, O., Hatcher, E., Venable, R.M., Pastor, R.W., MacKerell, A.D., Jr.: CHARMM additive all-atom force field for glycosidic linkages between hexopyranoses. J. Comput. Chem. (2009). https://doi.org/10.1021/ct900242e
38. Jorgensen, W.L., Chandrasekhar, J., Madura, J.D., Impey, R.W., Klein, M.L.: Comparison of simple potential functions for simulating liquid water. J. Chem. Phys. (1983). https://doi.org/10.1063/1.445869
39. Kuttel, M.M., Jackson, G.E., Mafata, M., Ravenscroft, N.: Capsular polysaccharide conformations in pneumococcal serotypes 19F and 19A. Carbohydr. Res. (2015). https://doi.org/10.1016/j.carres.2014.12.013
40. Kuttel, M.M., Ståhle, J., Widmalm, G.: CarbBuilder: Software for building molecular models of complex oligo-and polysaccharide structures. J. Comput. Chem. (2016). https://doi.org/10.1002/jcc.24428
41. Humphrey, W., Dalke, A., Schulten, K.: VMD: visual molecular dynamics. J. Mol. Graph. (1996). https://doi.org/10.1016/0263-7855(96)00018-5
42. Darden, T., York, D., Pedersen, L.: Particle mesh Ewald: An N·log (N) method for Ewald sums in large systems. J. Chem. Phys. (1993). https://doi.org/10.1063/1.464397
43. Van Gunsteren, W.F., Berendsen, H.J.: A leap-frog algorithm for stochastic dynamics. Mol. Simul. (1988). https://doi.org/10.1080/08927028808080941
44. Grossfield, A., Zuckerman, D.M.: Quantifying uncertainty and sampling quality in biomolecular simulations. Annu. Rep. Comput. Chem. (2009). https://doi.org/10.1016/S1574-1400(09)00502-7
45. Hunter, J.D.: Matplotlib: A 2D Graphics Environment (2007). https://doi.org/10.1109/MCSE.2007.55
46. Haltiwanger, R.S.: Symbol nomenclature for glycans (SNFG). Glycobiology (2016). https://doi.org/10.1093/glycob/cww005
47. Neelamegham, S., Aoki-Kinoshita, K., Bolton, E., Frank, M., Lisacek, F., Lütteke, T., O'Boyle, N., Packer, N.H., Stanley, P., Toukach, P.: Updates to the symbol nomenclature for glycans guidelines. Glycobiology (2019). https://doi.org/10.1093/glycob/cwz045
48. Hlozek, J., Kuttel, M.M., Ravenscroft, N.: Conformations of Neisseria meningitidis serogroup A and X polysaccharides: The effects of chain length and O-acetylation. Carbohydr. Res. (2018). https://doi.org/10.1016/j.carres.2018.06.007
49. Gracia Luis: WMC PhysBio Clustering (2012). Accessed June 2020

50. Cross, S., Kuttel, M.M., Stone, J.E., Gain, J.E.: Visualisation of cyclic and multi-branched molecules with VMD. J. Mol. Graph. Model. (2009). https://doi.org/10.1016/j.jmgm.2009.04.010
51. Krone, M., Stone, J.E., Ertl, T., Schulten, K.: Fast Visualization of Gaussian Density Surfaces for Molecular Dynamics and Particle System Trajectories., Vienna Austria (2012).
52. Zhang, S., Sella, M., Sianturi, J., Priegue, P., Shen, D., Seeberger, P.H.: Discovery of oligosaccharide antigens for semi-synthetic glycoconjugate vaccine leads against Streptococcus suis serotypes 2, 3, 9 and 14. Angew. Chem. Int. Ed. (2021). https://doi.org/10.1002/anie.202103990
53. Soeters, H.M., Oliver, S.E., Plumb, I.D., Blain, A.E., Zulz, T., Simons, B.C., Barnes, M., Farley, M.M., Harrison, L.H., Lynfield, R.: Epidemiology of Invasive Haemophilus influenzae Serotype a Disease—United States, 2008–2017. Clin. Infect. Dis. (2020). https://doi.org/10.1093/cid/ciaa875
54. Soeters, H.M., Blain, A., Pondo, T., Doman, B., Farley, M.M., Harrison, L.H., Lynfield, R., Miller, L., Petit, S., Reingold, A.: Current epidemiology and trends in invasive Haemophilus influenzae disease—United States, 2009–2015. Clin. Infect. Dis. (2018). https://doi.org/10.1093/cid/ciy187